Received: May 27, 2024; **Accepted:** July 15, 2024.
DOI. 10.30473/coam.2024.71425.1255
Summer-Autumn (2024) Vol. 9, No. 2, (97-121)
Research Article

Open Access

Control and Optimization in Applied Mathematics - COAM

A New Approach to Control of Legged Robots

Majid Anjidani

Department of Computer Engineering and Information Technology, Payame Noor University (PNU), Tehran, Iran.

Correspondence:
Majid Anjidani
E-mail:
m_anjidani@pnu.ac.ir

Abstract. Designing dynamically stable controllers for a robot with $2r$ legs is challenging due to its complex hybrid dynamics ($r > 1$). This paper proposes a technique to decompose the robot into r biped robots, where the influence of other robot parts on each biped can be modeled as external forces. This approach allows existing research on biped control to be applied to the quadruped robot. Time-invariant controllers, which typically ensure walking stability for planar point-footed bipeds, are selected for this purpose. For clarity, we focus on a planar point-footed quadruped for decomposition. We extend a recent reinforcement learning method to optimize these controller parameters for walking on slopes or under specific forces, while accounting for significant modeling errors in the quadruped. Simulation results demonstrate that our method achieves stable walking with the desired features and effectively compensates for modeling errors.

Keywords. Legged robots, Reinforcement learning, Gait optimization.

MSC. 90C34; 90C40.

How to Cite
Anjidani, M. (2024). "A new approach to control of legged robots", Control and Optimization in Applied Mathematics, 9(2): 97-121.

1 Introduction

There are several commercial and sociological motivations for researching legged robots, such as their deployment in dangerous situations[6], movement rehabilitation for the disabled [1, 12] . The control algorithms for legged robots can be categorized into time-dependent and time-invariant groups [33]. Time-dependent algorithms, depicted in Figure 1(a), are widely used. These include precomputed trajectory tracking methods [33], where trajectories generated by Central Pattern Generators (CPGs) [2, 3, 4, 24, 25] or length-varying inverted pendulums [19, 20, 21, 22, 23] dominate. Such algorithms often rely on principles like the Zero Moment Point (ZMP) criterion [18, 27, 28] which, however, do not guarantee stability [13, 33].

In contrast, few time-invariant control schemes have been proposed, as illustrated in Figure 1b. These controllers impose a set of holonomic constraints instead of tracking of precomputed trajectories [7, 8, 9, 10, 11, 14, 15, 16, 29, 30, 31, 32]. A distinct advantage of the proposed controller is its ability to induce backward walking by applying a sufficiently large external force in the opposite direction of forward motion [11], indicating that external forces primarily influence walking speed while still enforcing constraints [5].

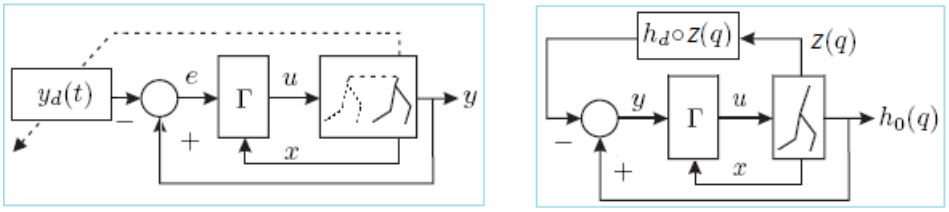

(a) A time-dependent controller block diagram: Designing trajectories, which results in stable, nonlinear, time-varying, closed-loop system, is challenging [33].

(b) A time-invariant controller block diagram [33].

Figure 1: Control of legged robots

Time-invariant controllers for quadruped robots have primarily focused on bounding motions [7, 8, 9], where front and back legs operate synchronously, effectively modeling the robot as a biped. However, considering all four legs introduce greater complexity, as the high-dimensional dynamics depend on the configuration of the supporting legs[1] [17]. Continuous dynamics can switch with changes in supporting legs, and discontinuities occur at the impact moments when legs touch the ground [17]. Consequently, designing a hybrid time-invariant controller for a quadruped or robots with even more legs presents significant challenges.

In this paper, we propose a method to decompose a robot with $2r$ legs into r biped robots. This is achieved by calculating the internal forces at the waist joints, allowing for a representation of the robot as r bipedal entities. Each biped part can then utilize a time-invariant controller for locomotion. As noted, external forces affect only walking speed, ensuring that constraints are enforced—the proposed controller is thus well-suited for this approach. This marks a novel utilization of time-invariant controllers in this context.

[1] A supporting leg is one that is in contact with the ground.

The method is demonstrated for planar robots with point-feet and specialized waist configurations, but it can be generalized to various other designs. Here, we consider the biped parts to also be planar with point-feet. Designing an exponentially stable walking gait to meet desired specifications—characterizing the holonomic constraints of the biped parts—is framed as a nonlinear optimization problem with constraints; solvable with existing numerical optimization tools [10, 11, 32, 33]. Additionally, an online Reinforcement Learning (RL) technique known as PI^2-WG has recently been introduced for gait design [5]. Three primary reasons motivate our use of PI^2-WG over traditional optimization methods. First, finding an initial gait for PI^2-WG is generally simpler than solving the optimization problem [5]. Second, this initial gait is more adaptable across various situations compared to the optimization framework [5]. Lastly, learning via PI^2-WG can continue to adjust for modeling errors present in real robots [5].

We also extend PI^2-WG for robots with $2r$ legs to design stable walking gaits incorporating desired characteristics. Simulation results indicate that the robot can learn to walk with specific speeds and postures in various environments, including surfaces with defined slopes and friction, while accounting for specific external forces and modeling errors. In Section 2, we introduce the robot decomposition process. Section 3 details the closed-loop dynamics of the biped parts, and Section 4 presents the RL method extension for the robot. Finally, Section 5 discusses simulation results.

2 Decomposition of the Robot with $2r$ Legs

In legged robots, the equations of continuous dynamics are determined based on the supporting legs. This means that the continuous dynamics will vary depending on which legs are in contact with the ground. Additionally, a discontinuity occurs at the moment a leg impacts the ground, leading to an increase in the complexity of the system's dynamics as more legs are added. Consequently, designing a hybrid time-invariant controller becomes increasingly complicated with the addition of more legs and the consequent discontinuities at contact.

To address this issue, we can compute the internal forces at the waist joints of a legged robot. The core idea is to treat the dynamics of the robot as a series of biped parts, where internal forces are represented as external forces acting on each biped component. Therefore, by applying external forces to the torso of these biped parts, we can utilize a time-invariant controller to manage the locomotion of the entire robot effectively.

We will formulate the dynamics of a planar quadruped with point feet, as illustrated in Figure 2. This approach isolates the dynamics of two biped parts, identified as Biped 1 and Biped 2, as well as the waist through the internal forces acting within the system. For simplicity, the waist configuration shown in Figure 2 is a linear rod, which can be modified for various waist designs. The two joints connecting the waist to the biped parts are considered to be non-actuated. The relationship between force and displacement in a linear rod behaves similarly to that of a spring as shown in Figure 3:

$$F = (EA/l)\, u,$$

where F represents the force (in Newton), and u denotes the displacement along the rod (in meters), which is the only direction of potential movement. The parameters E, A, M and l correspond to the

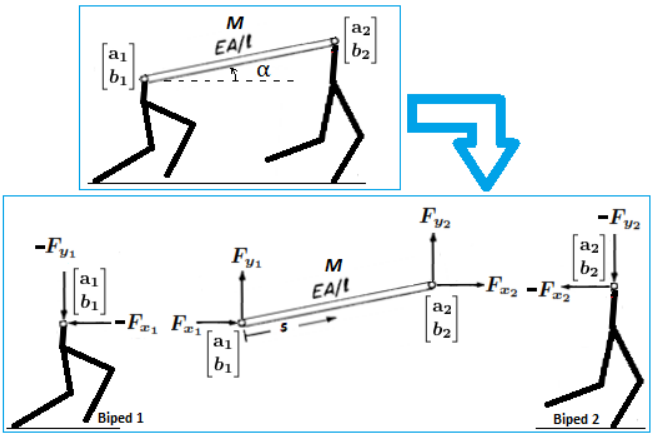

Figure 2: Quadruped decomposition to two biped robots and a waist.

modulus of elasticity (in N/m^2), cross-sectional area (in m^2), total mass (in kg), and free length (in meters) of the rod, respectively.

By adjusting the values of K_1, K_2, E, A, M, and l, we can fine-tune the waist configuration to achieve our desired design.

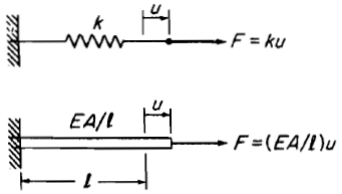

Figure 3: The relation of force and displacement for a rod [26].

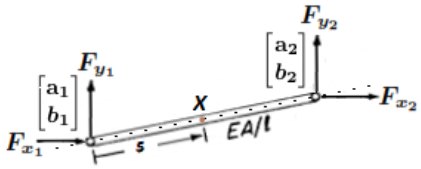

Figure 4: A rod with arbitrary planar motion.

Assuming that $[a_1;\ b_1]$ and $[a_2;\ b_2]$ represent the starting and ending points of a rod with a free length l along its central axis, as illustrated in Figure 4, the coordinate of a point X on the central axis can be expressed as follows:

$$X = \begin{bmatrix} \left(1 - \frac{s}{l}\right) a_1 + \frac{s}{l}\, a_2 \\ \left(1 - \frac{s}{l}\right) b_1 + \frac{s}{l}\, b_2 \end{bmatrix}, \tag{1}$$

where s represents the distance of point X from the starting point when the rod is in its free (unstressed) length, the displacement of X from its equilibrium position can be calculated as follows:

$$u = \frac{s}{l}\,(l - len)\,.$$

The length of the rod is given by the formula $len = \sqrt{(\mathrm{a}_2-\mathrm{a}_1)^2+(b_2-b_1)^2} = \sqrt{(\triangle \mathrm{a})^2+(\triangle b)^2}$ where $\triangle \mathrm{a}=\mathrm{a}_2-\mathrm{a}_1$ and $\triangle b=b_2-b_1$. Additionally, the waist angle α can be calculated using the formula $\alpha=\arctan(\triangle b/\triangle \mathrm{a})$.

According to Hooke's law, which states that $P/A=E\ du/ds$, the potential energy of the rod can be computed as follows [26]:

$$U = \frac{1}{2}\int_0^l AE\left(\frac{du}{ds}\right)^2 ds.$$

The total potential energy of the rod, taking into account the gravitational potential energy, is expressed as:

$$U = \frac{1}{2}\int_0^l AE\left(\frac{du}{ds}\right)^2 ds + \int_0^l mgh\ ds. \tag{2}$$

The total mass of the points on the cross-sectional area of the rod in X can be denoted as m. In this case, m equals M/l, where M is the total mass and l is the length of the rod. Additionally, the height h for point X is given by:

$$\left(1-\frac{s}{l}\right) b_1 + \frac{s}{l}\, b_2.$$

Therefore, the potential energy is computed as:

$$U = \frac{AE}{2l}(l-len)^2 + \frac{Mg}{2}(b_2+b_1),$$

and the kinetic energy of the rod is:

$$T = \frac{1}{2}m\int_0^l V^T V ds + \frac{1}{2}I\omega^2,$$

where $I = Mlen^2/12$ and $\omega = \dot{\alpha} = (\triangle \dot{b} \triangle \mathrm{a} - \triangle \dot{\mathrm{a}} \triangle b)/len^2$ and the velocity V of X according to (1) is:

$$V = \begin{bmatrix} \left(1-\frac{s}{l}\right)\dot{\mathrm{a}}_1 + \frac{s}{l}\dot{\mathrm{a}}_2 \\ \left(1-\frac{s}{l}\right)\dot{b}_1 + \frac{s}{l}\dot{b}_2 \end{bmatrix}.$$

Therefore, the kinetic energy after simplifying by Maple is:

$$T = \frac{M}{6}(\dot{\mathrm{a}}_1^2 + \dot{\mathrm{a}}_1\dot{\mathrm{a}}_2 + \dot{\mathrm{a}}_2^2 + \dot{b}_1^2 + \dot{b}_1\dot{b}_2 + \dot{b}_2^2) + \frac{M}{24}\frac{(\triangle b \triangle \dot{\mathrm{a}} - \triangle \mathrm{a} \triangle \dot{b})^2}{len^2}.$$

To derive the dynamic equations of the rod, we can employ the Lagrange equations. The Lagrangian is defined as the difference between kinetic and potential energy:

$$\begin{aligned} L = T - U = {} & \frac{M}{6}\left(\dot{\mathrm{a}}_1^2 + \dot{\mathrm{a}}_1\dot{\mathrm{a}}_2 + \dot{\mathrm{a}}_2^2 + \dot{b}_1^2\dot{b}_1\dot{b}_2 + \dot{b}_2^2\right) \\ & + \frac{M}{24}\frac{(\triangle b \triangle \dot{\mathrm{a}} - \triangle \mathrm{a} \triangle \dot{b})^2}{len^2} - \frac{AE}{2l}(l-len)^2 - \frac{Mg}{2}(b_2+b_1). \end{aligned}$$

The dynamics equations of the rod are:

$$\begin{aligned} &\frac{d}{dt}\frac{\partial L}{\partial \dot{\mathrm{a}}_1} - \frac{\partial L}{\partial \mathrm{a}_1} = F_{x_1}, \quad \frac{d}{dt}\frac{\partial L}{\partial \dot{\mathrm{a}}_2} - \frac{\partial L}{\partial \mathrm{a}_2} = F_{x_2}, \\ &\frac{d}{dt}\frac{\partial L}{\partial \dot{b}_1} - \frac{\partial L}{\partial b_1} = F_{y_1}, \quad \frac{d}{dt}\frac{\partial L}{\partial \dot{b}_2} - \frac{\partial L}{\partial b_2} = F_{y_2}. \end{aligned} \tag{3}$$

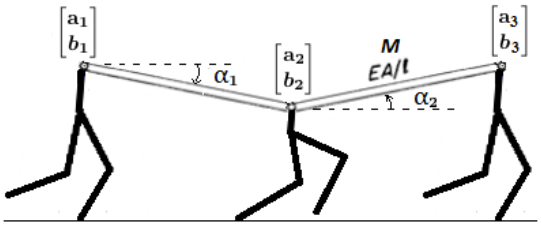

Figure 5: A robot with six legs can be decomposed to three biped robots and two waists.

Therefore, having $[a_1; b_1]$, $[\dot{a}_1; \dot{b}_1]$, $[\ddot{a}_1; \ddot{b}_1]$, $[a_2; b_2]$, $[\dot{a}_2; \dot{b}_2]$ and $[\ddot{a}_2; \ddot{b}_2]$, the internal forces $[F_{x_1}; F_{y_1}]$ and $[F_{x_2}; F_{y_2}]$ can be calculated using (3). It's important to note that $F_{ext1} = [-F_{x_1}; -F_{y_1}]$ represents the impact of Biped 2 and the waist on Biped 1, while $F_{ext2} = [-F_{x_2}; -F_{y_2}]$ represents the impact of Biped 1 and the waist on Biped 2. This method is also applicable to a robot with more legs. For instance, we can apply it to a robot with six legs, as depicted in Figure 5. The external force on the second biped is the cumulative force calculated from the dynamics equations of the two waists for the point $[a_2; b_2]$.

3 Closed-Loop System of Each Biped Part

In this paper, we have reformulated the close-loop hybrid dynamics model of point-footed planar biped robots [33] in order to specify the walking gait parameters that will be learned by a vector Θ. Consider the hybrid dynamics model for a planar point-footed biped robot as follows [33]:

$$\begin{cases} D(q)\ddot{q} + C(q,\dot{q}) + V(q) = \begin{bmatrix} u \\ 0 \end{bmatrix} - F_{fr}(q,\dot{q}) + J^T F_{ext}, & t \notin T_{impact}, \\ [q^+; \dot{q}^+] = \Delta([q^-; \dot{q}^-]), & t \in T_{impact}, \end{cases}$$

where $F_{fr}(q,\dot{q})$ represents the viscous and Coulomb friction torques. The matrix $D \in \Re^{n\times n}$ represents the inertia, $C \in \Re^{n\times n}$ represents the Coriolis and centripetal forces, and $V \in \Re^{n\times 1}$ denotes the forces due to gravity and elasticity. Additionally, $F_{fr} \in \Re^{n\times 1}$ represents the viscous and Coulomb friction torques, and $F_{ext} = [F_x;\ F_y]$ includes the external force and torque applied on the highest robot point.

Moreover, $J \in \Re^{n\times 2}$ represents the Jacobian matrix, where n represents the degree of freedom. The generalized coordinates are denoted as $q = [q_b; q_n]$, with $q_b = [q_1; \ldots; q_{n-1}]$ involving $n-1$ body coordinates and q_n representing the robot orientation with respect to the inertial frame. The control input is represented as $u = [u_1; \ldots; u_{n-1}] \in \Re^{n-1}$.

The set T_{impact} represents the possible impact moments, i.e., the ground impact times of the swing leg[1]. Furthermore, q^- and q^+ denote the generalized coordinates before and after the impact time, respectively. The role of two legs, either stance or swing, exchanges at this moment, and the state before impact $x^- = [q^-; \dot{q}^-]$ maps to the state after impact $x^+ = [q^+; \dot{q}^+]$ by the function $\triangle : \Re^{2n} \to \Re^{2n}$, thus marking the beginning of a new step. Therefore, the state space form can be formulated as follows:

[1] During walking, there are two main phases of locomotion: single support and double support. The single support phase occurs when only the stance foot is in contact with the ground, while the double support phase is when the swing foot makes contact with the ground and both feet are supporting the body.

$$\begin{cases} \dot{x} = f(x) + h(x)\,u, & t \notin T_{impact}, \\ x^{+} = \triangle(x^{-}), & t \in T_{impact}, \end{cases}$$

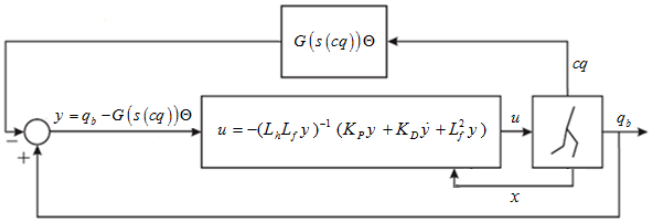

Figure 6: The closed-loop model of the biped robot.

where $x = [q; \dot{q}]$. and

$$f = \begin{bmatrix} \dot{q} \\ D^{-1}(q)(-C(q,\dot{q}) - V(q) - F_{fr}(q,\dot{q}) + J^{T} F_{ext}) \end{bmatrix},$$
$$h = \begin{bmatrix} 0_{n\times(n-1)} \\ D^{-1}(q)B \end{bmatrix}, \quad B = \begin{bmatrix} I_{(n-1)\times(n-1)} \\ 0_{1\times(n-1)} \end{bmatrix}.$$

The diagram in Figure 6 depicts the closed-loop system, with the control effort u being defined as follows [33]:

$$u = -(L_h L_f y)^{-1}(K_P y + K_D \dot{y} + L_f^2 y).$$

Here, L_h, L_f, and L_f^2 represent Lie derivatives. The gain matrices K_P and K_D are positive definite. $L_h L_f y$ is the decoupling matrix. Additionally, $y = q_b - q_{b,des}$, where the waking gait $q_{b,des}(z)$ is defined as:

$$q_{b,des}(z) = G(s(z))\Theta,$$

where $z = cq$ is a scalar where $c \in \Re^{1\times n}$ is a constant row vector ensuring that z has a monotonic change between $z^{+} = cq^{+}$ and $z^{-} = cq^{-}$ during a walking step [33]. Furthermore, $s(z) = (z - z_1)/(z_2 - z_1)$, where z_1 and z_2 are constant as defined in [5]. $G(s(z))$ and Θ are defined as:

$$G(s(z)) = \begin{bmatrix} \mathrm{g}(s(z))^{T} & & \mathrm{O} \\ & \ddots & \\ \mathrm{O} & & \mathrm{g}(s(z))^{T} \end{bmatrix},$$
$$\Theta = [\theta_1; \theta_2; \ldots; \theta_{n-1}], \quad \theta_d = \left[\theta_d^0; \theta_d^1; \ldots; \theta_d^L\right],$$

where vector $g(s(z)) \in \Re^{(L+1)}$ is defined by Bezier basis as:

$$g(s(z)) = \left[(1-s(z))^{L}; \ldots; \frac{L!\,s(z)^{m}(1-s(z))^{L-m}}{m!(L-m)!}; \ldots; s(z)^{L}\right],$$

Additionally, Θ encompasses the gait parameters that modify the virtual constraints $q_b - q_{b,des}(z) = 0$ imposed by the feedback controller. In essence, Θ includes the joint trajectory parameters (θ_d, $1 \leq$

$d \leq n-1$). Lastly, vector θ_d, representing the dth joint trajectory parameter, contains $L+1$ components ($\theta_d^m,\ 0 \leq m \leq L$). Therefore, the Bezier function of the trajectory of the dth joint is:

$$\mathrm{g}(s(z))^T \theta_d = \sum_{m=0}^{L} \theta_d^m \frac{L!}{m!\,(L-m)!} s(z)^m (1-s(z))^{L-m}.$$

Note that vector $\tilde{g}\,(z, \dot{z})$, which is used in the next section, is defined as [17]:

$$\tilde{g}(z,\dot{z}) \quad = \quad K_P g(s(z)) + K_D \frac{\dot{z}}{z_2 - z_1} \frac{\partial g(s(z))}{\partial s(z)} + \frac{\dot{z}^2}{(z_2 - z_1)^2} \frac{\partial^2 g(s(z))}{\partial s(z)^2}.$$

The stochastic closed-loop hybrid dynamics model can be expressed as follows:

$$\begin{cases} \dot{x} = f^{cl}\,(x, \Theta + \epsilon_t)\,, & t \notin T_{impact}, \\ x^+ = \triangle\,(x^-)\,, & t \in T_{impact}. \end{cases}$$

The exploration noise ϵ_t is defined as:

$$\epsilon_t = [\varepsilon_{1,t}; \varepsilon_{2,t}; \ldots; \varepsilon_{n-1,t}],$$

where $\varepsilon_{d,t}$ is the exploration noise vector drawn from a mean-zero multivariate Gaussian distribution with covariance Σ_d, and added to the shape parameter θ_d. To achieve an optimal Θ, the RL method PI^2-WG, which is presented in the next section, can be utilized.

4 Reinforcement Learning Method

PI^2-WG [17] is an RL algorithm designed to optimize the walking gait in a planar biped robot with point-feet having n degrees of freedom and 1 degree of underactuation. The pseudo-code of PI^2-WG can be found in Algorithm 1.

In PI^2-WG, exploration is managed by adding noise to the walking gait parameter vector $\Theta = [\theta_1; \ldots; \theta_{n-1}]$, where the vectors $\theta_1, \ldots, \theta_{n-1}$ represent the joint trajectory parameters. Essentially, K samples of $\theta_d,\ \ d = 1, \ldots, n-1$ are drawn from the multivariate normal distribution $N(\theta_d, \Sigma_d)$, resulting in K samples of Θ. The samples of Θ, denoted as $\Theta_k,\ k = 1, \ldots, K$, are then used to generate new rollouts starting from x_0, which are evaluated by a cost function. The vector Θ is updated by a weighted averaging of the parameter samples with regard to the cost of the generated rollouts in the Update function. In the Update function, $Q_{k,i}$ is an arbitrary state-dependent cost function at time t_i and $\phi_{k,N}$ is the final cost at time t_N of the kth rollout. Additionally, $S_{k,i}$ denotes the cost of the kth rollout after time t_i and $P_{k,i}$ represents the weight of the kth rollout after time t_i. Vector $\tilde{g}_{k,i}$ is equal to:

$$\tilde{g}_{k,i} = \tilde{g}(z_{k,i}, \dot{z}_{k,i}),$$

where $z_{k,i}$ and $\dot{z}_{k,i}$ denote the value of z and $\dot{z}$ at time t_i of the kth rollout.

Algorithm 1 PI^2-WG pseudo-code for point-footed planar biped robot

Given: Θ_{init}(i.e., $\theta_{d=1,\ldots,n-1,init}$), $\Sigma_{d=1,\ldots,n-1,init}, x_0$,

$K = 10, u = 0.$

Repeat

1. Generate_K_Rollouts (x_0,Θ) where $\Theta = [\theta_1, \ldots, \theta_{n-1}]$,
2. Update(Θ),
3. $u = u + 1.$

Until termination condition is satisfied

Generate_K_Rollouts (x_0, Θ)

1. For $k = 1, \ldots, K$ do
2. For $d = 1, \ldots, n-1$ do
3. $\theta_{d,k} \leftarrow N(\theta_d, \Sigma_d)$ where $\varepsilon_{d,k} = \theta_{d,k} - \theta_d$
4. $\Theta_k = [\theta_{1,k}; \ldots; \theta_{n-1,k}]$
5. $\tilde{g}_{k,i=0,\ldots,N-1},\ Q_{k,i=0,\ldots,N-1}, \phi_{k,N}$=Rollout$(x_0, \Theta_k)$

Update (Θ)

1. For $d = 1, \ldots, n-1$, $k = 1, \ldots, K$ and $i = 0, \ldots, N-1$ do:
2. $M_{d,k,i} = (R_d^{-1}\tilde{g}_{k,i}\tilde{g}_{k,i}^T)/(\tilde{g}_{k,i}^T R_d^{-1}\tilde{g}_{k,i})$
3. For $i = 0, \ldots, N-1$ do
4. For $k = 1, \ldots, K$ do
5. $S_{i,k} = \phi_{k,N} + \sum_{j=i}^{N-1} Q_{k,j}$
6. $+\frac{1}{2}\sum_{j=i}^{N-1}\sum_{d=1}^{n-1}(\theta_d + M_{d,k,j}\varepsilon_{d,k})^T R_d(\theta_d + M_{d,k,j}\varepsilon_{d,k})$
7. For $k = 1, \ldots, K$ do
8. $SN_{i,k} = 10\frac{S_{i,j} - \min_{j=1,\ldots,K} S_{i,j}}{\max_{j=1,\ldots,K} S_{i,j} - \min_{j=1,\ldots,K} S_{i,j}}$
9. $P_{i,k} = exp\,(-SN_{i,k}) \,/\, \sum_{j=1}^{K} exp\,(-SN_{i,k})$
10. For $d = 1, \ldots, n-1$ do
11. $\delta\theta_{d,i} = \sum_{k=1}^{K} P_{i,k} M_{d,k,i}\varepsilon_{d,k}$
12. For $d = 1, \ldots, n-1$ do
13. $\delta\theta_d = \left[\sum_{i=0}^{N-1} (N-i)\,\delta\theta_{d,i}\right] / \sum_{i=0}^{N-1} (N-i)$
14. $\theta_d = \theta_d + \delta\theta_d.$

Algorithm 2 PI^2-WG pseudo-code for point-footed planar quadruped robot

Given: Θ_{init}(i.e., $\theta_{d=1,\ldots,n-1,init}$), $\Sigma_{d=1,\ldots,n-1,init}$, x_0,

$K = 10, u = 0, x_0^{B1} = x_0^{B2} = x_0, \Theta^{B1}$=$\Theta^{B2}$=$\Theta_{init}$.

Repeat

1. Generate_K_Quadruped_Rollouts ($x_0^{B1}, x_0^{B2}, \Theta^{B1}, \Theta^{B2}$)

2. Update (Θ^{B1}, Θ^{B2}) %Θ^{B1}=$[\theta_1, \ldots, \theta_{n-1}]$, Θ^{B2}=$[\theta_n, \ldots, \theta_{2n-2}]$

3. $u = u + 1$

Until termination condition is satisfied

Generate_K_Quadruped_Rollouts ($\boldsymbol{x_0^{B1}, x_0^{B2}, \Theta^{B1}, \Theta^{B2}}$)

1. For $k = 1, \ldots, K$ do:
2. For $d = 1, \ldots, 2n-2$ do
3. $\theta_{d,k} \leftarrow N(\theta_d, \Sigma_d)$
5. $\Theta_k^{B1} = [\theta_{1,k}; \ldots; \theta_{n-1,k}]$
6. | $\Theta_k^{B2} = [\theta_{n,k}; \ldots; \theta_{2n-2,k}]$
7. | Generate_Quadruped_Rollout ($x_0^{B1}, x_0^{B2}, \Theta_k^{B1}, \Theta_k^{B2}$)

Generate_Quadruped_Rollout ($\boldsymbol{x_0^{B1}, x_0^{B2}, \Theta_k^{B1}, \Theta_k^{B2}}$)

Initial state of Biped 1 = x_0^{B1},

Initial state of Biped 2 = x_0^{B2},

Initial forces of the bipeds: $F_{ext1} = F_{ext2} = [0; -Mg/2]$.

1. For $i = 0, \ldots, N-1$ do
2. $[q_{B1}; \dot{q}_{B1}; \ddot{q}_{B1}]$=nextState(Closed-loop equation of Biped 1 (Θ_k^{B1})),
3. $[q_{B2}; \dot{q}_{B2}; \ddot{q}_{B2}]$=nextState(Closed-loop equation of Biped 2 (Θ_k^{B2})),
4. $[a_1; b_1]$, $[\dot{a}_1; \dot{b}_1]$ and $[\ddot{a}_1; \ddot{b}_1]$ = Torso_end_point ($q_{B1}, \dot{q}_{B1}, \ddot{q}_{B1}$),
5. $[a_2; b_2]$, $[\dot{a}_2; \dot{b}_2]$ and $[\ddot{a}_2; \ddot{b}_2]$ = Torso_end_point ($q_{B2}, \dot{q}_{B2}, \ddot{q}_{B2}$),
6. Compute F_{ext1} and F_{ext2} according to (3),
7. Compute $\tilde{g}_{k,i}^{B1}$, $\tilde{g}_{k,i}^{B2}$, $Q_{k,i}^{B1}$, $Q_{k,N}^{B2}$, $\phi_{k,i}^{B1}$, and $\phi_{k,N}^{B2}$.

Update($\boldsymbol{\Theta^{B1}, \Theta^{B2}}$)

1. For $k = 1, \ldots, K$ and $i = 0, \ldots, N-1$ do
2. For $d = 1, \ldots, n-1$ do
3. $M_{d,k,i} = [R_d^{-1}\tilde{g}_{k,i}^{B2}(\tilde{g}_{k,i}^{B2})^T]/[(\tilde{g}_{k,i}^{B2})^T R_d^{-1}\tilde{g}_{k,i}^{B2}]$
4. For $d = n, \ldots, 2n-2$ do
5. $M_{d,k,i} = [R_d^{-1}\tilde{g}_{k,i}^{B1}(\tilde{g}_{k,i}^{B1})^T]/[(\tilde{g}_{k,i}^{B1})^T R_d^{-1}\tilde{g}_{k,i}^{B1}]$
6. For $i = 0, \ldots, N-1$ do
7. For $k = 1, \ldots, K$ do
8. $S_{i,k} = (\phi_{k,N}^{B1} + \phi_{k,N}^{B2}) + \sum_{j=i}^{N-1}(Q_{k,i}^{B1} + Q_{k,i}^{B2}) + \frac{1}{2}\sum_{j=i}^{N-1}\sum_{d=1}^{2n-2}(\theta_d + M_{d,k,j}\varepsilon_{d,k})^T R_d(\theta_d + M_{d,k,j}\varepsilon_{d,k})$
9. For $k = 1, \ldots, K$ do
10. $SN_{i,k} = 10\frac{S_{i,j} - \min_{j=1,\ldots,K} S_{i,j}}{\max_{j=1,\ldots,K} S_{i,j} - \min_{j=1,\ldots,K} S_{i,j}}$
11. $P_{i,k} = exp(-SN_{i,k}) / \sum_{j=1}^{K} exp(-SN_{i,k})$
12. For $d = 1, \ldots, 2n-2$ do
13. $\delta\theta_{d,i} = \sum_{k=1}^{K} P_{i,k} M_{d,k,i}\varepsilon_{d,k}$
14. For $d = 1, \ldots, 2n-2$ do
15. $\delta\theta_d = \left[\sum_{i=0}^{N-1}(N-i)\,\delta\theta_{d,i}\right] / \sum_{i=0}^{N-1}(N-i)$
16. $\theta_d = \theta_d + \delta\theta_d$

4.1 Extending PI^2-WG for a Robot with r Biped Parts

Algorithm 2 contains the pseudo-code of the extended PI^2-WG for the quadruped robot, considering the decomposition done in the previous section. The function Generate_Quadruped_Rollout is utilized to generate a rollout for the quadruped robot. Within the function, $q, \dot{q}$, and $\ddot{q}$ are renamed to $q_{B1}, \dot{q}_{B1}$, and $\ddot{q}_{B1}$ for Biped 1, and are renamed to $q_{B2}, \dot{q}_{B2}$, and $\ddot{q}_{B2}$ for Biped 2. The function Torso_end_point calculates the position and acceleration of a point on the torso of the biped parts that are connected to the waist, while the function Rotational_spring_angles computes the angles between the waist and the torsos. It is important to note that we use the index $d\in[1,\ldots,2n-2]$ for the quadruped joints, with $d\in[1,\ldots,n-1]$ denoting the joint index of Biped 1 and $d\in[n,\ldots,2n-2]$ denoting the joint index of Biped 2. Therefore, we denote the walking gait parameters of Biped 1 and Biped 2 as $\Theta^{B1}=[\theta_1,\ldots,\theta_{n-1}]$ and $\Theta^{B2}=[\theta_n,\ldots,\theta_{2n-2}]$ respectively. It is important to note that the following cost function is used for the quadruped in the Update function:

$$\begin{aligned} S_{i,k} &= (\phi^{B1}_{k,N}+\phi^{B2}_{k,N})+\sum_{j=i}^{N-1}(Q^{B1}_{k,i}+Q^{B2}_{k,i}) \\ &\quad +\frac{1}{2}\sum_{j=i}^{N-1}\sum_{d=1}^{2n-2}(\theta_d+M_{d,k,j}\varepsilon_{d,k})^T R_d(\theta_d+M_{d,k,j}\varepsilon_{d,k}), \end{aligned}$$

The immediate costs, i.e., $\phi^{B1}_{k,N}$ and $\phi^{B2}_{k,N}$, and the final costs, i.e., $Q^{B1}_{k,i}$ and $Q^{B2}_{k,i}$ of the biped parts are defined the same as $\phi_{k,N}$ and $Q_{k,j}$ for a biped robot in PI^2-WG [17]. By this approach, the parameters Θ^{B1} and Θ^{B2} can be optimized in the closed-loop systems of the biped parts, resulting in good quadruped locomotion. PI^2-WG can be similarly extended for a robot with $2r$ legs, in which case the cost function is:

$$\begin{aligned} S_{i,k} &= \sum_{p=1}^{r}\phi^{B_p}_{k,N}+\sum_{j=i}^{N-1}\sum_{p=1}^{r}Q^{B_p}_{k,i} \\ &\quad +\frac{1}{2}\sum_{j=i}^{N-1}\sum_{d=1}^{rn-r}(\theta_d+M_{d,k,j}\varepsilon_{d,k})^T R_d(\theta_d+M_{d,k,j}\varepsilon_{d,k}), \end{aligned}$$

where B_p denotes the pth biped part.

5 Result

This section examines the performance of the proposed method on a simulated model of the quadruped as discussed in the previous section. The waist parameters are adjusted as detailed in Table 1. Both bipeds parts share the same model parameters, which are outlined in the Appendix. The extended PI^2-WG aims to enhance the quadruped locomotion. The values of Σ_d, where $d=1,\ldots,4$, are specified in [17] as follows:

$$\Sigma_1=2\rho I,\quad \Sigma_2=3\rho I,\quad \Sigma_3=\rho I,\quad \Sigma_4=5\rho I,$$

where the initial value of ρ is provided in Table 3. In each scenario, 1500 updates are executed, and ρ is uniformly reduced over 1000 updates to a value of 0.0001, and subsequently set to $\rho=0.0001$.

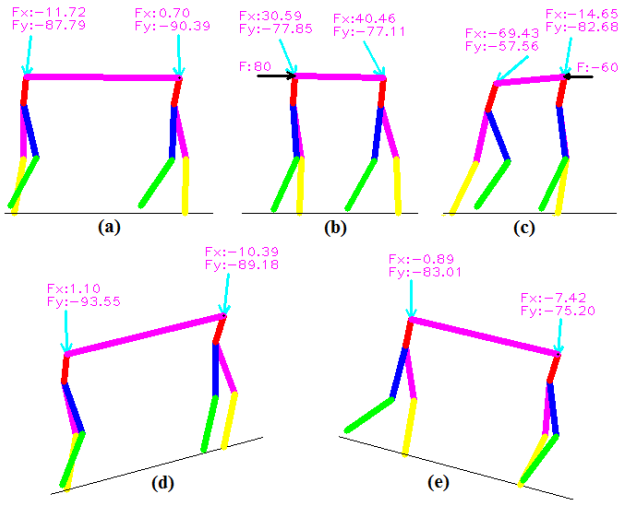

Figure 7: The quadruped's locomotion is evaluated in several specific scenarios: (a) Flat surface, (b) Flat surface with a horizontal external force of 80 N exerted indefinitely, (c) Flat surface with a horizontal external force of -60 N exerted indefinitely, (d) 15-degree slope, and (e) -15-degree slope. The blue arrows illustrate the internal forces at the two waist joints in each scenario.

Table 1: Waist parameters of the quadruped

E	A	l	M
100000	0.001	1.1	20

Figure 7 depicts various walking postures achieved using gaits designed by extended PI^2-WG for the quadruped in different scenarios. The blue arrows above the torso of the biped parts represent internal forces, while the black arrow indicates an external force applied to the quadruped. The yellow link denotes the stance leg's tibia, and the green link represents the swing leg's tibia of the biped parts. Although the robot initially struggles to walk even a single step with the initial gait (4) according to Remark 2 in the Appendix, it demonstrates improved walking ability after the learning process.

Table 2: The features for designed gaits

Gait	Scenario	Biped part	μ^a_{req}	A^b	B^c
G1	Flat	Biped 1	0.594	0.0206	62
G1	Flat	Biped 2	0.50333	0.0219	61.6
G2	Flat with E1	Biped 1	0.72239	0.0379	69
G2	Flat with E1	Biped 2	0. 669	0.0371	65
G3	Force -60 N	Biped 1	0. 6977	0.0109	120.7
G3	Force -60 N	Biped 2	0.6186	0.0817	109.1
G4	Force -60 N with E2	Biped 1	0.4132	0.0012	134
G4	Force -60 N with E2	Biped 2	0.40325	0.0188	65.2
G5	Force 80 N	Biped 1	0.6293	0.0422	131.9
G5	Force 80 N	Biped 2	0.5575	0.0403	140.9
G6	Force 80 N with E2	Biped 1	0.361	0.0038	143.3
G6	Force 80 N with E2	Biped 2	0.424	0.0108	133.7
G7	Slope -15	Biped 1	0.5435	0.0031	136.7
G7	Slope -15	Biped 2	0. 5069	0.0009	131.1
G8	Slope -15 with E3	Biped 1	0.5818	0.0423	131.7
G8	Slope -15 with E3	Biped 2	0.5608	0.0338	124.6
G9	Slope 15	Biped 1	0.7379	0.0028	120.9
G9	Slope 15	Biped 2	0.6569	0.0196	140
G10	Slope 15 with E3	Biped 1	0.8159	0.0152	142.7
G10	Slope 15 with E3	Biped 2	0.6952	0.0026	122.7

μ^a_{req}: Required friction coefficient of the ground,

A^b: Absolute difference between last step speed and the desired speed,

B^c: Pick torque (Nm) [17].

Table 3: Initial value of ρ

Learned gait	ρ
G1, G2, G5, and G6	0.01
G3, G4, G7, and G8	0.02
G9 and G10	0.001

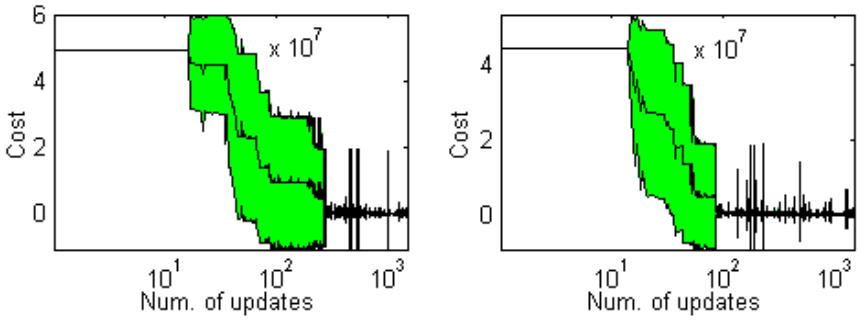

Figure 8: Learning curve for Left: G1, Right: G2.

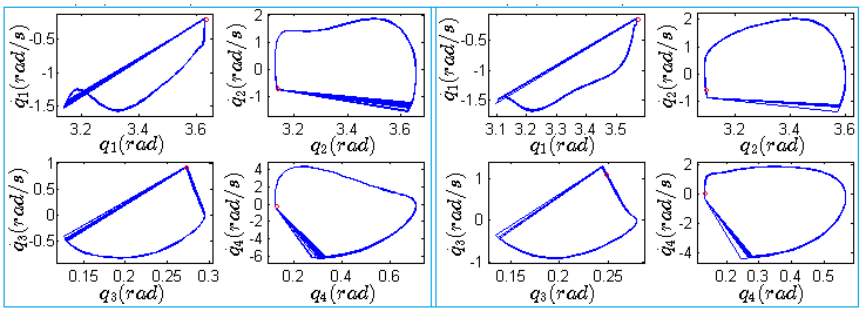

Figure 9: The phase portraits of 100 walking steps by G1. Left: Biped 1, Right: Biped 2.

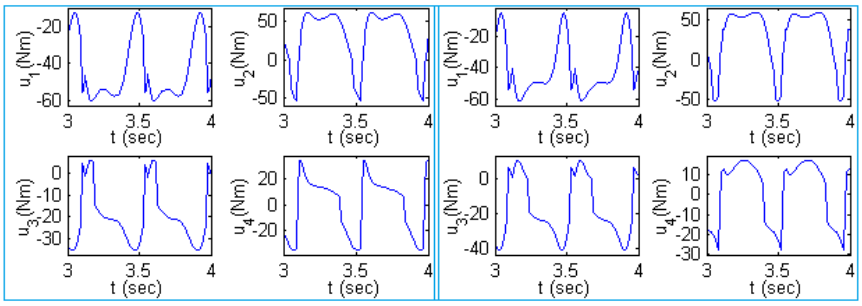

Figure 10: The torques applied in time interval [3s, 4s] during walking by G1. Left: Biped 1, Right: Biped 2.

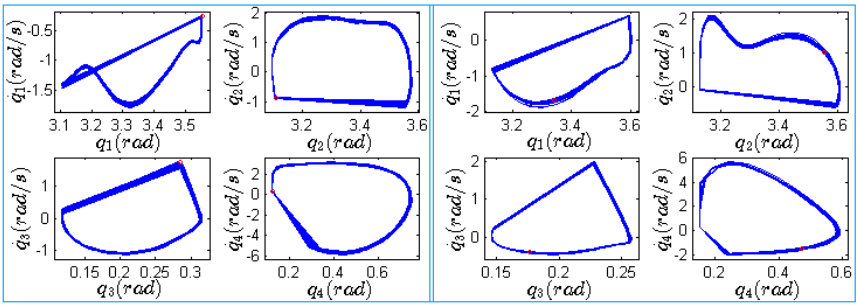

Figure 11: The phase portraits of 100 walking steps by G2. Left: Biped 1, Right: Biped 2.

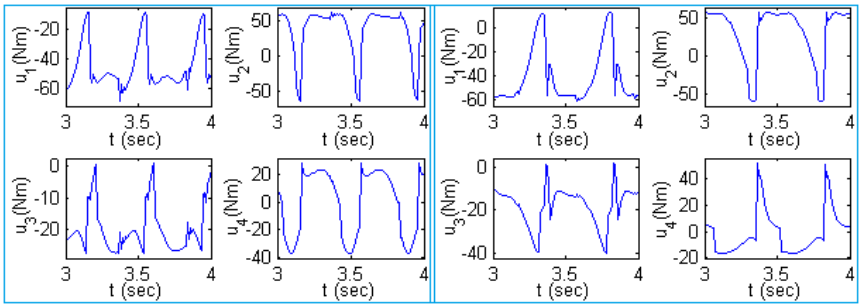

Figure 12: The torques applied in time interval [3s, 4s] during walking by G2. Left: Biped 1, Right: Biped 2.

The parameters of the quadruped's waist are outlined in Table 1. Table 2 provides the features of example gaits generated by the extended PI^2-WG under various conditions. The symbol μ_{req} represents the necessary friction coefficient of the ground for the biped components. Column B specifies the maximum torque for the biped joints, which must not exceed 150 Nm.

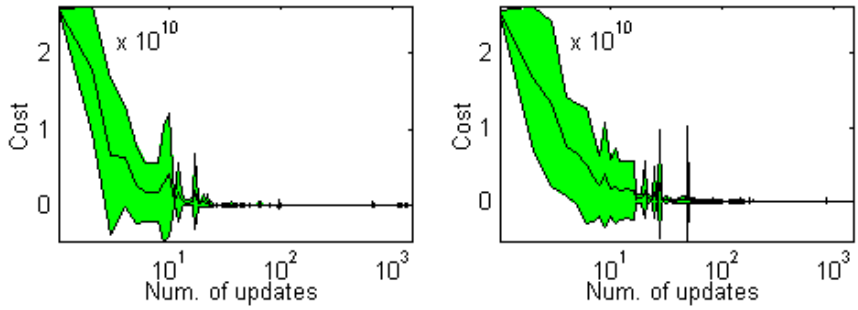

Figure 13: Learning curve for Left: G3, Right: G4.

The results show that using extended PI^2-WG, the robot is capable of learning to walk with desired features in the scenarios even considering a large modeling error in feedback controller design.

Remark 1. The ability of large modeling error compensation is a feature of the RL method to continue the learning with the real robot which is not possible by an offline optimization.

The data presented in Table 2 indicates that the robot successfully learned to walk on a flat surface with static friction of 0.75, even in the presence of external forces -60 N or 80 N and modeling errors E1-

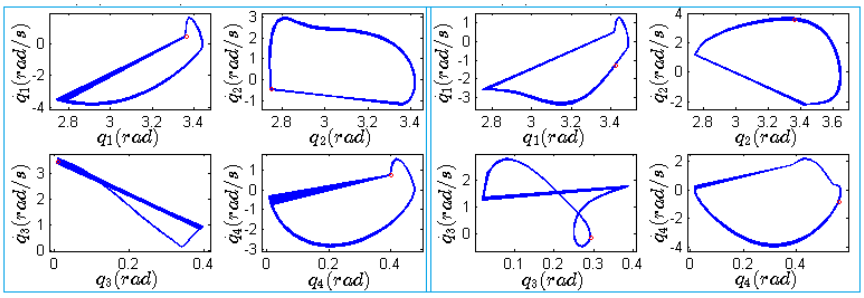

Figure 14: The phase portraits of 100 walking steps by G3. Left: Biped 1, Right: Biped 2.

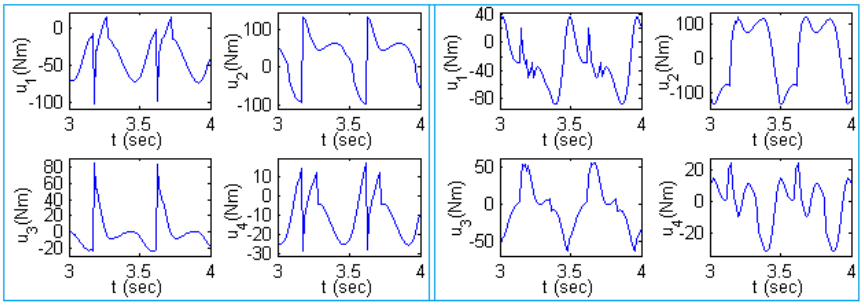

Figure 15: The torques applied in time interval $[3s, 4s]$ during walking by G3. Left: Biped 1, Right: Biped 2.

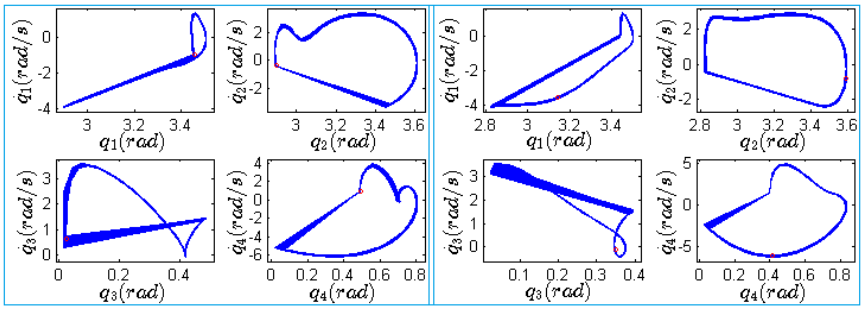

Figure 16: The phase portraits of 100 walking steps by G4. Left: Biped 1, Right: Biped 2.

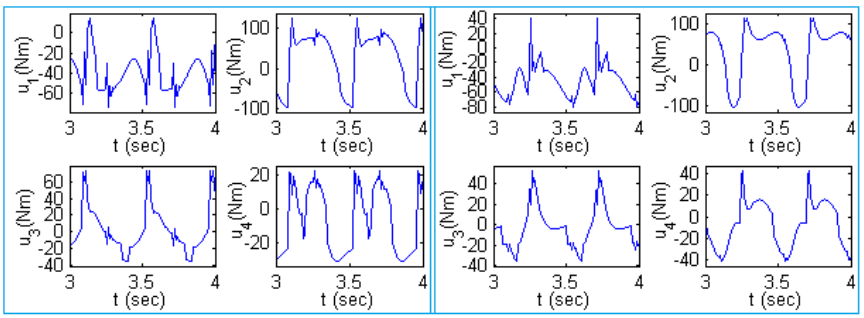

Figure 17: The torques applied in time interval $[3s, 4s]$ during walking by G4. Left: Biped 1, Right: Biped 2.

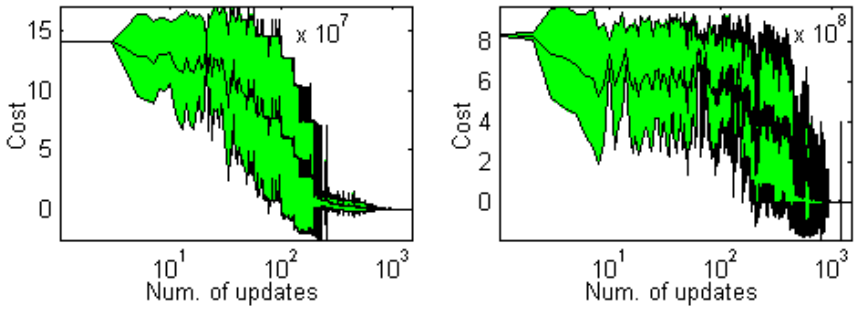

Figure 18: Learning curve for Left: G5, Right: G6.

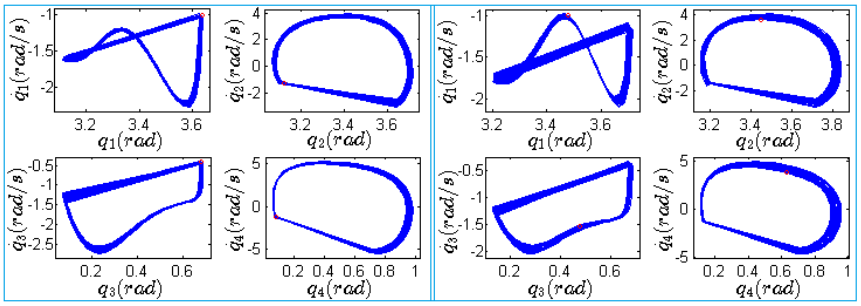

Figure 19: The phase portraits of 100 walking steps by G5. Left: Biped 1, Right: Biped 2.

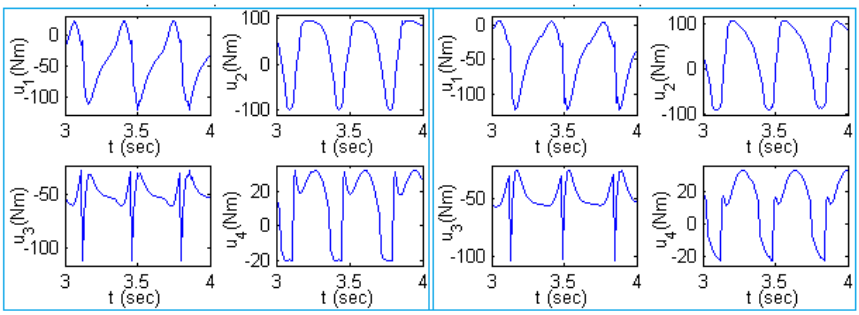

Figure 20: The torques applied in time interval $[3s, 4s]$ during walking by G5. Left: Biped 1, Right: Biped 2.

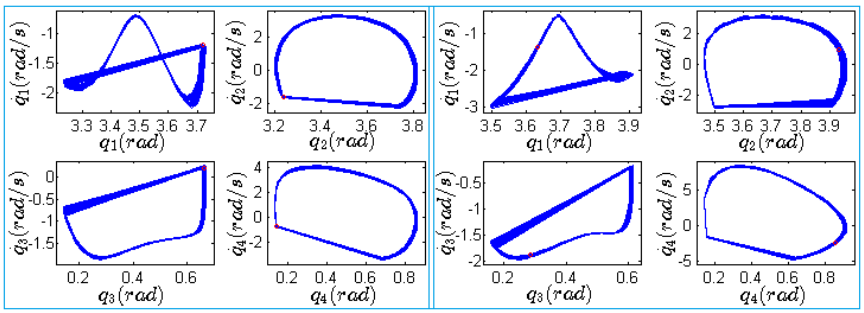

Figure 21: The phase portraits of 100 walking steps by G6. Left: Biped 1, Right: Biped 2.

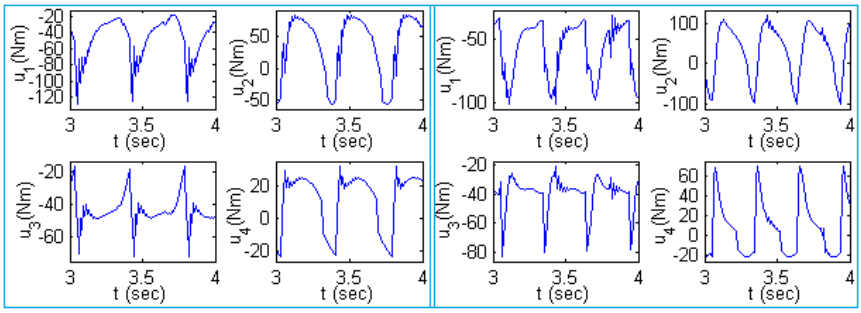

Figure 22: The torques applied in time interval $[3s, 4s]$ during walking by G6. Left: Biped 1, Right: Biped 2.

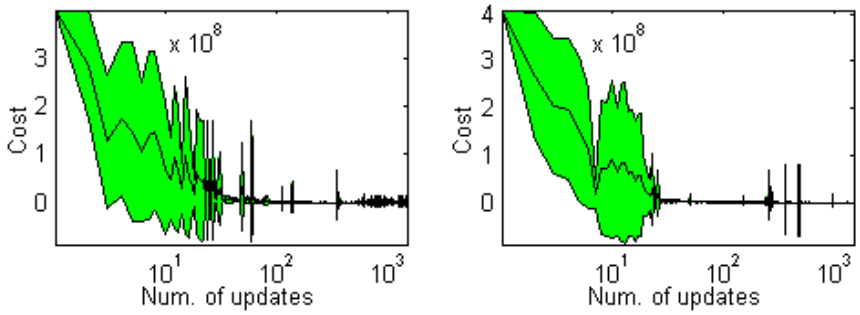

Figure 23: Learning curve for Left: G7, Right: G8.

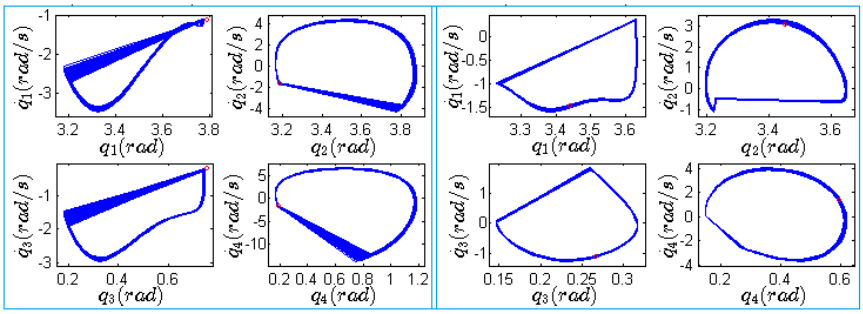

Figure 24: The phase portraits of 100 walking steps by G7. Left: Biped 1, Right: Biped 2.

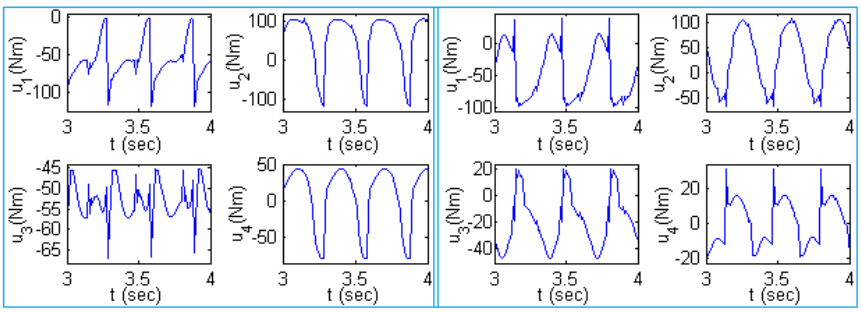

Figure 25: The torques applied in time interval $[3s, 4s]$ during walking by G7. Left: Biped 1, Right: Biped 2.

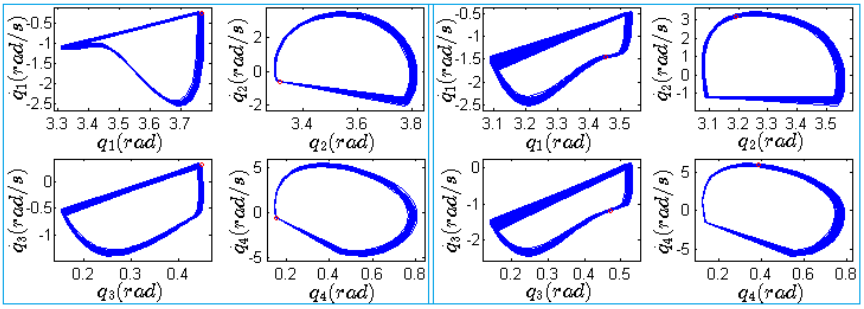

Figure 26: The phase portraits of 100 walking steps by G8. Left: Biped 1, Right: Biped 2.

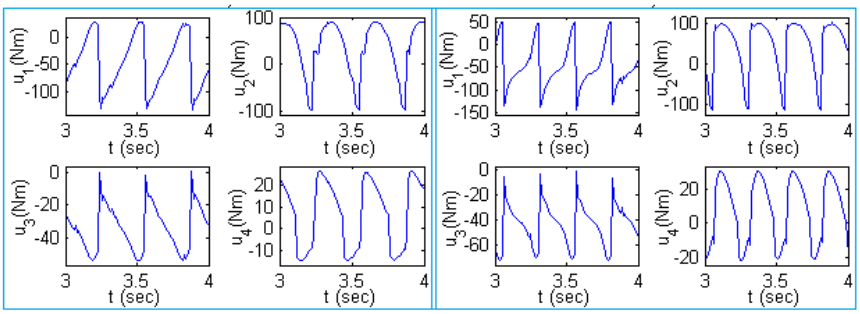

Figure 27: The torques applied in time interval $[3s, 4s]$ during walking by G8. Left: Biped 1, Right: Biped 2.

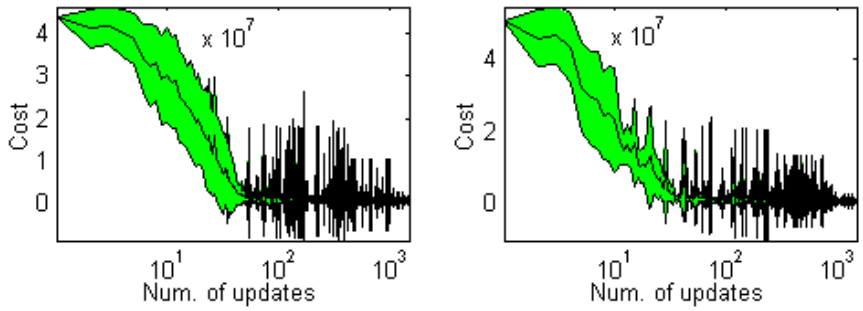

Figure 28: Learning curve for Left: G9, Right: G10.

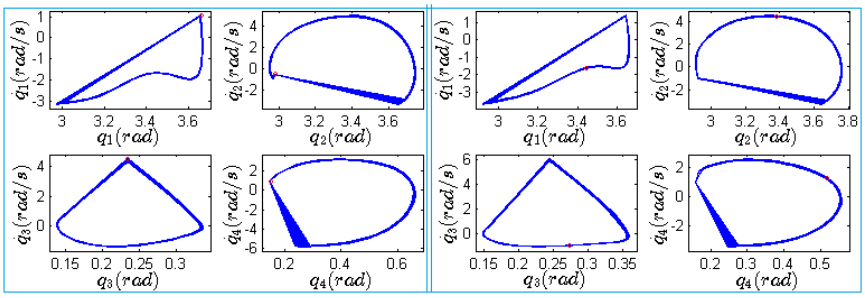

Figure 29: The phase portraits of 100 walking steps by G9. Left: Biped 1, Right: Biped 2.

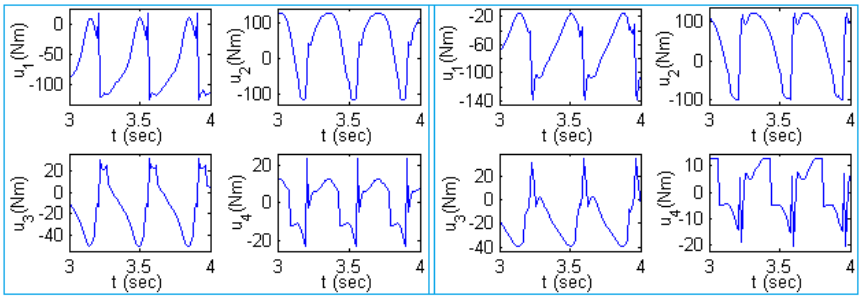

Figure 30: The torques applied in time interval $[3s, 4s]$ during walking by G9. Left: Biped 1, Right: Biped 2.

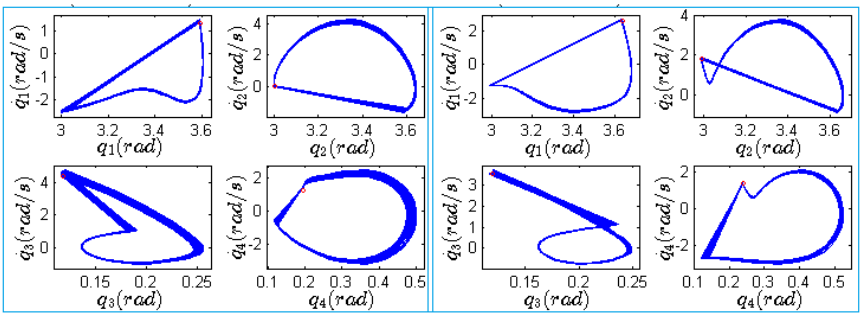

Figure 31: The phase portraits of 100 walking steps by G10. Left: Biped 1, Right: Biped 2.

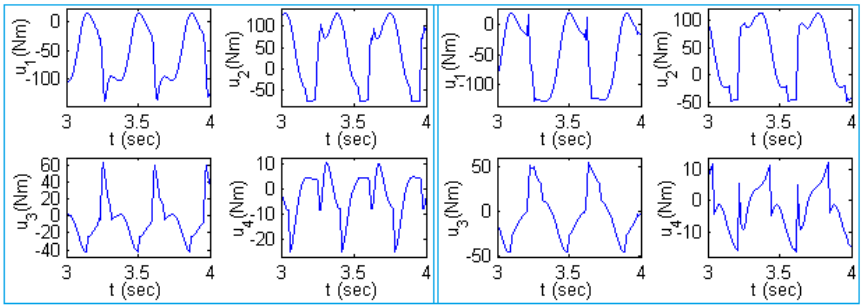

Figure 32: The torques applied in time interval $[3s, 4s]$ during walking by G10. Left: Biped 1, Right: Biped 2.

E2 (refer to Table 5 in the Appendix). Additionally, the table demonstrates the robot's ability to walk on a slope of -15 degrees with static friction of 0.6, despite the presence of modeling error E3. Furthermore, it shows that walking on a slope of 15 degrees is achievable, even in the presence of modeling error E3.

Figures 8, 13, 18, 23, and 28 showcase the average learning curves derived from 10 runs of extended PI^2-WG in various scenarios with/without modeling error. These curves depict the progress over iterations of extended PI^2-WG. Moreover, the phase portraits in Figures 9, 11, 14, 16, 19, 21, 24, 26, 29, and 31 illustrate the designed gaits of the different scenarios with/without modeling error for 100 walking steps. The red circle in the figures represents the robot's initial state. Figures 10, 12, 15, 17, 20, 22, 25, 27, 30, and 32 display the motor torques during walking with the designed gait in the different scenarios.

6 Conclusion

In this paper, the proposed technique for decomposing a robot with $2r$ legs into r biped robots has been presented. The effects of the other robot parts on each biped can be represented as external forces. The results section includes a consideration of a planar point-footed quadruped robot for decomposition to simplify the explanation of the idea. An extension of a recent reinforcement learning method has been utilized to optimize the time-invariant controller parameters for walking with specific features on a certain slope or in the presence of a certain force, considering a large error in the model of the quadruped robot. The simulation results indicate that the proposed method achieves stable walking with desired features and quickly compensates for modeling errors. Future exploration includes the potential use of a camera sensor for adapting to real-time changes in the environment, such as detecting the slope of the surface and selecting a suitable walking gait previously learned for the encountered slope. Additionally, future work will aim to extend the method for 3D motions, as the robot motions in this paper are currently limited to planar motions.

Appendix: RABBIT and PARAMETERS

RABBIT is a point-footed robot with 5 degrees of freedom ($n = 5$) and planar motions[33]. Its model parameters can be found in Table 4. Figure 23 displays the robot and its associated model parameters. For detailed information on RABBIT modeling and the computation of ground reaction forces, please refer to [33]. The equations of motion for RABBIT can be produced using MATLAB code, which can be accessed at the provided https://web.eecs.umich.edu/~grizzle/biped_book_web/

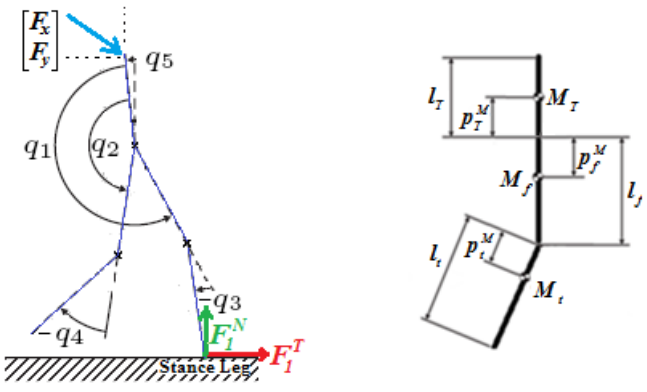

(a) Generalized coordinates for the biped robot.

(b) Link length and center of mass position [33].

Figure 33: The robot and its associated model parameters

In early rollouts of the learning, RABBIT starts walking with the initial state $x_0 = [q_0; \dot{q}_0]$ where q_0 and $\dot{q}_0$ are:

$$q_0 = [3.2741; 3.4364; 0.1701; 0.6643; -0.012],$$

$$\dot{q}_0 = [-1.5344; 2.0201; -0.2029; 0.0244; 0].$$

The row vector c is set to c=$[-1; 0; -0.5; 0; -1]^T$. The initial Θ is set as (the unit of the numbers is radian):

$$\Theta = [\theta_1; \theta_2; \ldots; \theta_{n-1}] \tag{4}$$

$$\theta_1 = \begin{bmatrix} 3.47 \\ 3.294 \\ 3.399 \\ 2.947 \end{bmatrix}, \quad \theta_2 = \begin{bmatrix} 2.934 \\ 3.606 \\ 3.62 \\ 3.445 \end{bmatrix}, \quad \theta_3 = \begin{bmatrix} 0.1962 \\ 0.1712 \\ 0.153 \\ 0.115 \end{bmatrix}, \quad \theta_4 = \begin{bmatrix} 0.1258 \\ 1.147 \\ 0.3627 \\ 0.2013 \end{bmatrix}.$$

Except for the flat scenario, the initial Θ is used in all scenarios.

Table 4: The value for parameters which is illustrated in Figure 23

link parameter	**Value**
Mass (kg)	M_T=12, M_f=6.8, M_t=3.2
Inertia (kgm^2)	$I_T = 0.33$, $I_f = 0.47$, $I_t = 0.2$
Length (m)	$l_T = 0.2$, $l_f = 0.4$, $l_t = 0.4$
Center (m)	p_T^M=0.1, p_f^M=0.11, p_t^M=0.24

Table 5: Errors considered for model parameters

No.	$\boldsymbol{M_T}$	$\boldsymbol{I_T}$	$\boldsymbol{l_T}$	$\boldsymbol{p_T^M}$	$\boldsymbol{M_f}$	$\boldsymbol{I_f}$	$\boldsymbol{l_f}$	$\boldsymbol{p_f^M}$	$\boldsymbol{M_t}$	$\boldsymbol{I_t}$	$\boldsymbol{l_t}$	$\boldsymbol{p_t^M}$
E1	-0.4	0.4	-0.01	0.1	-0.4	0.4	-0.01	0.1	0.4	-0.4	0.01	0.1
E2	0.4	-0.4	0.01	-0.1	0.4	-0.4	0.01	0.1	-0.4	-0.4	0.01	-0.1
E3	0.4	0.4	0.01	-0.1	-0.4	0.4	0.01	0.1	-0.4	0.4	0.01	-0.1

Remark 2. In the test phase, even one successful step is not possible by the initial gait (4) because the torque and friction limitation are considered. Note that for the learning phase, we have considered,

1. No saturation.
2. An unreal and very large fiction coefficient for the surface.

Therefore in the learning phase of all the scenarios, the robot is usually able to walk at least one successful step with the initial Θ.

The time step is $dt = 0.01$ [1]. The gains of PD for feedback controller are considered as:

[1]Note that we use a smaller time resolution at impact. At impact, we use $dt = 0.001$ in the learning phase and $dt = 0.0001$ in the test phase.

$$K_P = 500I_{(n-1)\times(n-1)}, K_D = 50I_{(n-1)\times(n-1)}.$$

The joint friction which is compensated by the controller is:

$$F_{fr}(q, \dot{q}) = F_v\dot{q} + F_s sgn(\dot{q}).$$

where the coefficients in viscous and Coulomb friction terms are considered as:

$$F_v = \text{diag}(16.5, 16.5, 5.48, 5.48, 0),$$
$$F_s = \text{diag}(15, 15, 8.84, 8.84, 0).$$

Table 5 includes three modeling errors. They are applied to the model parameters to specify the effects of modeling errors on the RL algorithm performance.

Declarations

Availability of Supporting Data

All data generated or analyzed during this study are included in this published paper.

Funding

The authors conducted this research without any funding, grants, or support.

Competing Interests

The authors declare that they have no competing interests relevant to the content of this paper.

References

[1] Agarwal, P., Kuo, P.H., Neptune, R.R., Deshpande, A.D. (2013). "A novel framework for virtual prototyping of rehabilitation exoskeletons", IEEE International Conference on Rehabilitation Robotics.

[2] Ajallooeian, M., Pouya, S., Sproewitz, A., Ijspeert, A. (2013). "Central pattern generators augmented with virtual model control for quadruped rough terrain locomotion", IEEE International Conference on Robotics and Automation.

[3] Ajallooeian, M., Gay, S., Tuleu, A., Sprowitz, A., Ijspeert, A.J. (2013). "Modular control of limit cycle locomotion over unperceived rough terrain", IEEE/RSJ International Conference on Intelligent Robots and Systems, IROS.

[4] Ajallooeian, M., Pouya, S., Gay, S., Tuleu, A., Sprowitz, A., Ijspeert, A. (2013). "Towards modular control for moderately fast locomotion over unperceived rough terrain", Dynamic Walking.

[5] Anjidani, M., Jahed Motlagh, M.R., Fathy, M., Nili Ahmadabadi, M. (2019). "A novel online gait optimization approach for biped robots with point-feet", ESAIM: Control, Optimisation and Calculus of Variations, 25(81).

[6] Baudoin, Y. Habib, M.K. (2011). "Using robots in hazardous environments: Landmine detection, de-mining and other applications", Woodhead Publishing Limited.

[7] Cao, Q., Poulakakis, I. (2013). "Quadrupedal bounding with a segmented flexible torso: Passive stability and feedback control", Bioinspiration & Biomimetics, 8(4), 046007.

[8] Cao, Q., Poulakakis, I. (2014). "On the energetics of quadrupedal bounding with and without torso compliance", IEEE/RSJ International Conference on Intelligent Robots and Systems, 4901-4906.

[9] Cao, Q., Poulakakis, I. (2015). "On the energetics of quadrupedal running: Predicting the metabolic cost of transport via a flexible-torso model", Bioinspiration & Biomimetics, 10(5), 056008.

[10] Chevallereau, C., Westervelt, E.R., Grizzle, J.W. (2005). "Asymptotically stable running for a five-link, four-actuator, planar bipedal robot", International Journal of Robotics Research, 24, 431-464.

[11] Chevallereau, C., Abba, G., Aoustin, Y., Plestan, F., Westervelt, E.R., Canudas-de-Wit, C., Grizzle, J.W. (2003). "RABBIT: A testbed for advanced control theory", IEEE Control Systems Magazine, Paper number CSM-02-038.

[12] Dellon, B., Matsuoka, Y. (2007). "Prosthetics, exoskeletons, and rehabilitation", IEEE Robotics & Automation Magazine.

[13] Goswami, A. (1999). "Postural stability of biped robots and the foot-rotation indicator (FRI) point", International Journal of Robotics Research, 18(7), 523-33.

[14] Grizzle, J.W., Abba, G., Plestan, F. (1999). "Proving asymptotic stability of a walking cycle for a five DOF biped robot model", International Conference on Climbing and Walking Robots, 69-81.

[15] Grizzle, J.W., Abba, G., Plestan, F. (2001). "Asymptotically stable walking for biped robots: Analysis via systems with impulse effects", IEEE Transactions on Automatic Control, 46, 51-64.

[16] Grizzle, J.W., Plestan, F., Abba, G. (1999). "Poincare's method for systems with impulse effects: Application to mechanical biped locomotion", IEEE International Conference on Decision and Control, Phoenix, AZ.

[17] Hardt, M., Stryk, O.V. (2000). "Towards optimal hybrid control solutions for gait patterns of a quadruped", CLAWAR 2000 - 3rd International Conference on Climbing and Walking Robots, Madrid.

[18] Hirai, K., Hirose, M., Haikawa, Y., Takenake, T. (1998). "The development of Honda humanoid robot", IEEE International Conference on Robotics and Automation, Leuven, Belgium, 1321-1326.

[19] Kajita, S., Tani, K. (1996). "Experimental study of biped dynamic walking", IEEE Control Systems Magazine, 16(1), 9-13.

[20] Kajita, S., Yamaura, T., Kobayashi, A. (1992). "Dynamic walking control of biped robot along a potential energy conserving orbit", IEEE Transactions on Robotics and Automation, 8(4), 431-437.

[21] Kajita, S., Kanehiro, F., Kaneko, K., Yokoi, K., Hirukawa, H. (2001). "The 3D linear inverted pendulum mode: A simple modeling for a biped walking pattern generation", IEEE/RSJ International Conference on Intelligent Robots and Systems, Maui, HI, 239-246.

[22] Kajita, S., Kanehiro, F., Kaneko, K., Fujiwara, K., Yokoi, K., Hirukawa, H. (2002). "A realtime pattern generator for biped walking", IEEE International Conference on Robotics and Automation, Washington, D.C.

[23] Park, J.H., Kim, E.S. (2009). "Foot and body control of biped robots to walk on irregularly protruded uneven surfaces", Systems, Man, and Cybernetics, Part B: Cybernetics, IEEE Transactions on, 39(1), 289-297.

[24] Sugimoto, N., Morimoto, J. (2011). "Phase-dependent trajectory optimization for CPG-based biped walking using path integral reinforcement learning", 11th IEEE-RAS International Conference on Humanoid Robots, Bled, Slovenia, 26-28.

[25] Taga, G. (1995). "A model of the neuro-musculo-skeletal system for human locomotion II: Real-time adaptability under various constraints", Biological Cybernetics, 73, 113-121.

[26] Thomson, W.T., Dahleh, M.D. (1998). "Theory of Vibration with Applications", Fifth Edition, Prentice Hall, Copyright.

[27] Vukobratovic, M., Borovac, B. (2004). "Zero-moment point–thirty five years of its life", International Journal of Humanoid Robotics, 1(1), 157-73.

[28] Vukobratovic, M., Borovac, B., Surla, D., Stokic, D. (1990). "Biped Locomotion", Springer-Verlag, Berlin.

[29] Westervelt, E.R., Buche, G., Grizzle, J.W. (2004). "Experimental validation of a framework for the design of controllers that induce stable walking in planar bipeds", International Journal of Robotics Research, 23(7), 559-82.

[30] Westervelt, E.R., Buche, G., Grizzle, J.W. (2004). "Inducing dynamically stable walking in an under actuated prototype planar biped", IEEE International Conference on Robotics and Automation, New Orleans, LA, 4234-9.

[31] Westervelt, E.R., Grizzle, J.W., Canudas, C. (2003). "Switching and PI control of walking motions of planar biped walkers", IEEE Transactions on Automatic Control, 48(2), 308-12.

[32] Westervelt, E.R., Grizzle, J.W., Koditschek, D.E. (2003). "Hybrid zero dynamics of planar biped walkers", IEEE Transactions on Automatic Control, 48(1), 42-56.

[33] Westervelt, E.R., Grizzle, J.W., Chevallereau, Ch., Choi, J.H., Morris, B. (2007). "Feedback control of dynamic bipedal robot locomotion", CRC Press, Taylor & Francis Group.